Protocol for suppression of noise from stimulated multiphoton emissions in concatenated entanglement swapping links and quantum repeaters

Yousef K. Chahine [ID],[*] Ian R. Nemitz, and John D. Lekki
NASA Glenn Research Center, Cleveland, Ohio 44135, USA

Multiphoton emissions constitute a fundamental source of noise in quantum repeaters and other quantum communication protocols when probabilistic photon sources are employed. In this paper it is shown that by alternating the Bell state measurement basis in concatenated entanglement swapping links one can automatically identify and discard many errors from stimulated multiphoton emissions. The proposed protocol is shown to completely eliminate the dominant quadratic growth of multiphoton errors with the length of the repeater chain. Furthermore, it is shown that the protocol can be employed in satellite-assisted entanglement distribution links to enable links which are more robust in the presence of imbalanced channel losses. The analysis introduces a convenient calculus based on Clifford algebra for modeling concatenated entanglement swapping links with multiphoton emissions. In particular, we present a compact expression for the fidelity of the Bell state produced by a repeater chain of arbitrary length including noise from double-pair emissions.

I. INTRODUCTION

The ability to establish shared quantum systems exhibiting entanglement between remote locations has a growing number of potential applications, including quantum clock synchronization [1,2], distributed quantum sensing [3,4], and experimental tests of fundamental physics in new regimes [5]. The quantum repeater protocol enables the distribution of entangled states over long distances by concatenating elementary links using entanglement swapping. In this work we study repeater protocols with minimal quantum processing including probabilistic Bell state measurements (BSMs), quantum memories, and multiplexing with active mode switching across spatial, spectral, or temporal modes [6–9].

It was shown in [8] that multipair emissions can severely limit useful application of parametric down-conversion (PDC) sources in such a repeater architecture. Photon-number-resolving (PNR) detectors can be employed to overcome this limitation [10]; however, effective PNR requires highly efficient repeaters, since any photon losses between multiphoton production and detection limit the ability of the detector to identify multiphoton emissions. In this paper we introduce an alternating Bell state measurement (ABSM) protocol for further mitigating multiphoton noise in concatenated entanglement swapping links employing PDC sources which does not rely on PNR detection. The protocol exploits correlations in the two-mode squeezed vacuum (TMSV) state to automatically identify stimulated double-pair emissions at adjacent BSMs. The ABSM protocol thus alleviates the impact of imperfect PNR caused by inefficiencies between the source and linear optical BSM. In particular, it is shown in Sec. IV that the ABSM protocol eliminates the dominant quadratic

contribution to the growth of multiphoton errors in extended repeater chains with PDC sources.

The ABSM protocol also mitigates the increase in multiphoton noise in elementary links with imbalanced channel losses (Secs. IV and V). Imbalanced channels result from practical limitations and are unavoidable for satellite-assisted links and dynamic links where the locations of source nodes, BSM nodes, and repeater stations are constrained. If probabilistic photon sources are employed, the multiphoton emissions from one source can dominate the BSM, requiring attenuation of the source closer to the BSM to reduce the number double pairs. This additional attenuation effectively rebalances the channel losses at the cost of a reduction in link efficiency. In Sec. IV it is shown that the fidelity of the Bell state produced using the ABSM protocol is more robust to imbalanced losses. Furthermore, the ABSM protocol can be used in conjunction with multiplexed cascaded PDC sources [11] to further suppress double pairs in imbalanced entanglement swapping links (Sec. V).

The suppression of multiphoton noise is also important for concatenation of elementary links employing a Duan-Lukin-Cirac-Zoller (DLCZ)–type protocol using atomic ensembles [7,12,13]. Sources based on atomic ensembles produce entangled states exhibiting bosonic excitation statistics with a Hamiltonian formally identical to that of PDC [7] and thus can suffer the same types of multiphoton errors when employed in a quantum repeater chain. However, various DLCZ-type protocols based on two-photon interference include an additional detection entangling the emissions from several atomic ensembles leading to a more complex form for the multiphoton term, the analysis of which is beyond the scope of this work [12].

The ABSM protocol is presented in Sec. II, where it is shown that by employing alternating measurement bases in the linear optical BSMs, a stimulated double-pair emission
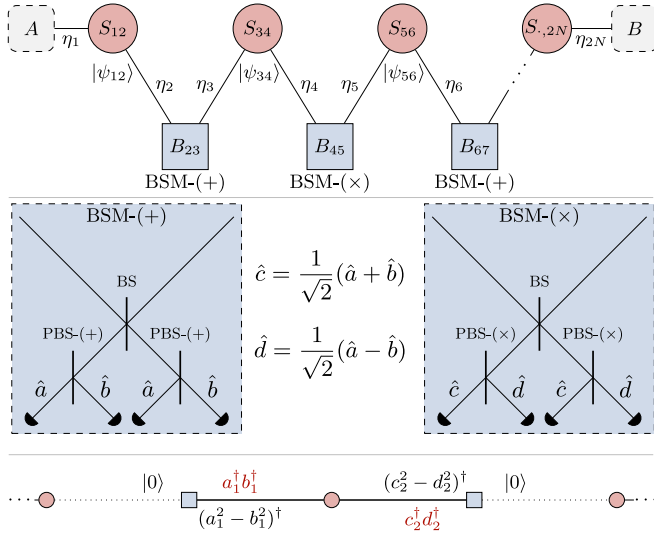

FIG. 1. Protocol for concatenated entanglement swapping links. Red circles denote entangled pair sources S_{ij} and blue squares denote Bell state analyzers B_{ij}. Channels are labeled by the corresponding transmission efficiency η_i. By alternating the BSM measurement basis, a double-pair emission from a single source S cannot trigger two adjacent BSMs.

from a single source cannot falsely trigger two adjacent BSMs. The resulting suppression of multiphoton errors is analyzed in Sec. IV, where it is shown that these errors constitute the dominant source of noise in extended quantum repeater chains using probabilistic sources, growing quadratically with the number of elementary links ℓ using the standard repeater protocol. The analysis is based on a new calculus introduced in Sec. III for key observables of the quantum state produced by repeater chains including multiphoton terms, enabling a closed-form expression for the Bell state fidelity produced by a repeater chain of arbitrary length. This simplifies the analysis compared to other approaches based on the Wigner formalism for Gaussian states [14] or numerical density-matrix calculations [8,15]. Other potential applications of the ABSM protocol for satellite-assisted entanglement distribution are discussed in Sec. V.

II. ALTERNATING BSM PROTOCOL

The protocol is based on the observation that the four-photon emission in a polarization-entangled TMSV state exhibits certain correlations between the two-photon states emitted into each output channel [16,17]. Specifically, the measurement of a two-photon state with orthogonal polarizations in one output channel is correlated to a two-photon state with correlated polarizations in the opposite channel when measured in a diagonal basis (4). Since a linear optical BSM requires detection of two photons with opposite polarizations, by alternating the measurement basis in a concatenated entanglement swap, a four-photon emission from a single source cannot independently trigger two adjacent BSMs (Fig. 1).

To make this rigorous, we express the entangled photon state, representing a pair of dual-rail qubits in a superposition of modes with bosonic annihilation operators $\{a_1, b_1\}$ and

$\{a_2, b_2\}$, in the form [8,18]

$$
\begin{aligned}
|\psi_{12}\rangle = \sqrt{p_{12}^{(0)}}|0\rangle &+ \sqrt{p_{12}^{(1)}/2}(a_1 b_2 - b_1 a_2)^\dagger |0\rangle \\
&+ \sqrt{p_{12}^{(2)}/12}(a_1^2 b_2^2 + b_1^2 a_2^2 - 2a_1 b_1 a_2 b_2)^\dagger |0\rangle,
\end{aligned}
\tag{1}
$$

where we have truncated higher-order terms in order to focus on the lowest-order contribution to the multiphoton error. This form for the entangled pair state is a tensor product of two copies of a TMSV state derived from the Hamiltonian for a PDC process. For the full TMSV state, the probability $p_{12}^{(n)}$ of producing n pairs is given by

$$
p_{12}^{(n)} = (n+1)(1 - |\lambda|^2)^2 |\lambda|^{2n},
\tag{2}
$$

where the parameter $|\lambda|^2 \ll 1$ determines the single-pair emission probability $p_{12} \equiv p_{12}^{(1)} \simeq 2|\lambda|^2$. In order to normalize the truncated state without changing the relation between single- and double-pair emissions, we set $p_{12}^{(0)} = 1 - p_{12}^{(1)} - p_{12}^{(2)}$. This normalization relies on the double-pair term to represent the multiphoton noise and results in a small overestimation of the vacuum component which subsumes the contribution from higher-order photon emissions [11].

Correlations in the four-photon term arise from the stimulated emission process captured in the bosonic relation $a^\dagger |n\rangle = \sqrt{n+1}|n+1\rangle$, which leads to a suppressed mixed term

$$
|2, 0; 0, 2\rangle + |0, 2; 2, 0\rangle - |1, 1; 1, 1\rangle
\tag{3}
$$

when written in the basis of Fock states $|m_1, n_1; m_2, n_2\rangle$ in modes $\{a_1, b_1, a_2, b_2\}$. A less obvious correlation is found by expanding the state of modes $\{a_2, b_2\}$ in the diagonal basis of $c_2 = \sqrt{1/2}(a_2 + b_2)$ and $d_2 = \sqrt{1/2}(a_2 - b_2)$ to obtain the four-photon term in the form

$$
\begin{aligned}
(a_1^2)^\dagger (c_2^2 + d_2^2 - 2c_2 d_2)^\dagger |0\rangle &+ (b_1^2)^\dagger (c_2^2 + d_2^2 + 2c_2 d_2)^\dagger |0\rangle \\
&- 2(a_1 b_1)^\dagger (c_2^2 - d_2^2)^\dagger |0\rangle.
\end{aligned}
\tag{4}
$$

The key property is that a measurement of opposite polarizations a_1 and b_1 in the first channel projects the state in the second channel onto a correlated two-photon NOON state in modes c_2 and d_2 (and vice versa).

One can exploit this correlation in a concatenated entanglement swap by noting that a linear optical BSM between two adjacent sources $|\psi_{12}\rangle|\psi_{34}\rangle$ only succeeds if opposite polarizations are detected. Furthermore, the BSM can be performed in either basis, as follows from the easily verified relations

$$
|\Psi^+\rangle_{ab} = |\Phi^-\rangle_{cd}, \qquad |\Phi^+\rangle_{ab} = |\Phi^+\rangle_{cd},
\tag{5}
$$

$$
|\Psi^-\rangle_{ab} = -|\Psi^-\rangle_{cd}, \qquad |\Phi^-\rangle_{ab} = |\Psi^+\rangle_{cd},
\tag{6}
$$

where

$$
|\Psi^\pm_{ij}\rangle_{ab} = \sqrt{\tfrac{1}{2}}(a_i^\dagger b_j^\dagger \pm b_i^\dagger a_j^\dagger)|0\rangle,
\tag{7}
$$

$$
|\Phi^\pm_{ij}\rangle_{ab} = \sqrt{\tfrac{1}{2}}(a_i^\dagger a_j^\dagger \pm b_i^\dagger b_j^\dagger)|0\rangle
\tag{8}
$$

represent the dual-rail Bell states in the $\{a, b\}$ basis, with analogous expressions for the representation in the $\{c, d\}$ basis. Thus, by performing adjacent Bell state measurements in concatenated entanglement swapping links in alternating diagonal bases, as illustrated in Fig. 1, the correlations observed in (4) ensure that a multipair emission cannot independently trigger a BSM in two adjacent Bell state analyzers.

Two important caveats are immediately apparent. First, the protocol relies on the correlations in the multiphoton state described by (1). Results presented in [17] give experimental justification for this form for the four-photon term, although source impurities allowing emission of each photon into more than two modes may degrade the correlations in the double-pair emissions. For example, if the secondary photon pair is emitted into a set of orthogonal modes $\{a'_1, b'_1, a'_2, b'_2\}$ (e.g., an adjacent temporal mode), then the required correlations do not exist. However, this is not a problem in practice since any implementation of the elementary entanglement swapping link must already filter out adjacent-mode noise in order to ensure the single-pair emissions yield indistinguishable photons at the beam-splitter where the BSM is performed. A more fundamental limitation of the protocol is the fact that it does not suppress multiphoton errors when one of the photons in the double-pair state is lost. In this case, the chain can still be corrupted if a photon from an adjacent source arrives at the BSM where the secondary emission was lost, although this type of error can still yield a Bell state with 75% fidelity [cf. Eq. (21)]. In Secs. IV and V it is shown that the protocol nevertheless provides significant multiphoton error mitigation for extended repeater chains as well as for elementary links with imbalanced losses.

III. CONCATENATED LINK MODEL

In order to analyze the noise suppression and gain afforded by the ABSM protocol we model a concatenated entanglement swapping link as shown in Fig. 1. We assume completely dephasing, pure-loss bosonic channels $a_i = e^{i\phi}\sqrt{\eta_i}a'_i + \sqrt{1 - \eta_i}a''_i$ with transmission efficiency η_i, where ϕ is a random phase accumulated equally on modes a_i and b_i. For simplicity, we assume that the external channels connecting the sources S_{12} and $S_{2N-1,2N}$ to the receivers at A and B are lossless $\eta_1 = \eta_{2N} = 1$. Detection in each linear optical BSM is modeled via the detector positive-operator-valued measure (POVM) including PNR as in [10]; however, to simplify the analysis we neglect extrinsic noise (i.e., we assume no background or dark counts). For all interior channels $\eta_2, \dots, \eta_{2N-1}$ the detection efficiency can be grouped with the channel transmission efficiency; the justification for this combined efficiency is an equivalence of quantum operations discussed in the Supplemental Material (SM) [19]. The detector POVMs are combined to form a single POVM consisting of the four possible successful outcomes from a chain of nominally successful BSMs, corresponding to the states $|\Psi_{AB}^{\pm}\rangle$ or $|\Phi_{AB}^{\pm}\rangle$, together with the complementary outcome representing failure of the link. Note that if all of the sources produce the state $|\psi_{ij}\rangle$ corresponding to $|\Psi_{ij}^{-}\rangle_{ab}$, then the nonalternating BSM protocol will only produce outcomes corresponding to $|\Psi_{AB}^{-}\rangle$ at the output of the full concatenated link; however, it

follows from (5) and (6) that all four outcomes are possible when employing the ABSM protocol.

The following analysis is based on the truncated state (1) which neglects three-pair emissions. Without the ABSM protocol, the probability of a three-pair error is always dominated by that of a corresponding two-pair error such that the three-pair error represents a small additional error of order $p_{ij} \ll 1$ relative to the two-pair error. Thus, the three-pair emissions only become relevant in cases where the ABSM protocol achieves suppression of a single source of two-pair errors by a factor approaching the pair generation probability p_{ij}. Since the ABSM protocol does not identify errors when at least one of the photons in a double pair is lost, this level of suppression only occurs in special situations with certain asymmetric channel losses which are identified in the following analysis.

We now develop the expression for the link efficiency and Bell state fidelity for a passively concatenated link; at the end of the section we discuss how these results directly generalize to concatenated links with simple quantum memories and active mode switching as in a quantum repeater architecture. The derivations are technical and are given in the SM [19]; in this section we simply present the resulting expressions for the link efficiency and Bell state fidelity used to model the performance of a concatenated entanglement swapping link with and without the ABSM protocol.

The efficiency of a $(2N - 2)$-fold coincidence yielding a chain of $N - 1$ successful BSMs in a passively concatenated link with N independent sources can be written

$$\bar{\eta}_{1,2N} = \sum_{\vec{v} \in \{0,1,2\}^N} p^{(\vec{v})} \beta^{(\vec{v})}, \tag{9}$$

where the sum is taken over all ternary sequences $\vec{v} = (v_1, v_2, \dots, v_N)$ in $\{0, 1, 2\}^N$ representing the number of pairs emitted by each source and

$$p^{(\vec{v})} = \prod_{i=1}^{N} p_{2i-1,2i}^{(v_i)}. \tag{10}$$

The expression (9) arises from a decomposition of the density matrix via Fock space projections in the input modes indexed by $\vec{v}$. The coefficients $\beta^{(\vec{v})}$ can be interpreted as the probability of a full chain of successful BSM outcomes if the ith source produces v_i photon pairs. Note that since we model sources coupled directly to completely dephasing channels, there are no coherent interference effects between states with distinct total photon number from each source (i.e., all off-diagonal density-matrix elements between such basis states vanish), and so we may speak unambiguously about the number of photons emitted by each source, subject only to our lack of knowledge of the number of photons emitted in a classical sense (see the SM [19]).

The coefficients $\beta^{(\vec{v})}$ can be written as a product of coefficients $\beta_{ij}^{(m,n)}$ describing the individual success probability of each BSM B_{ij} when m photons are emitted into channel i and n photons are emitted into channel j, respectively; however, there is some subtlety to the calculation since neighboring BSMs are correlated by the shared photon source. These correlations can be accounted for by defining the Clifford

numbers

$$\boldsymbol{\beta}_{ij}^{(1,1)} = \frac{1}{2}\eta_i\eta_j, \tag{11}$$

$$\boldsymbol{\beta}_{ij}^{(2,0)} = \frac{\boldsymbol{\sigma}_{i-1,i}}{3}\eta_i^2, \tag{12}$$

$$\boldsymbol{\beta}_{ij}^{(0,2)} = \frac{\boldsymbol{\sigma}_{j,j+1}}{3}\eta_j^2, \tag{13}$$

$$\boldsymbol{\beta}_{ij}^{(2,1)} = \eta_i\eta_j(1-\eta_i) + \frac{\boldsymbol{\sigma}_{i-1,i}}{3}\eta_i^2(1-\eta_j), \tag{14}$$

$$\boldsymbol{\beta}_{ij}^{(1,2)} = \eta_i\eta_j(1-\eta_j) + \frac{\boldsymbol{\sigma}_{j,j+1}}{3}\eta_j^2(1-\eta_i), \tag{15}$$

$$\boldsymbol{\beta}_{ij}^{(2,2)} = 2\eta_i\eta_j(1-\eta_i)(1-\eta_j)$$
$$+ \frac{\boldsymbol{\sigma}_{i-1,i}}{3}\eta_i^2(1-\eta_j)^2 + \frac{\boldsymbol{\sigma}_{j,j+1}}{3}\eta_j^2(1-\eta_i)^2, \tag{16}$$

$$\boldsymbol{\beta}_{ij}^{(0,0)} = \boldsymbol{\beta}_{ij}^{(0,1)} = \boldsymbol{\beta}_{ij}^{(1,0)} = 0,$$

where we have introduced abstract vector quantities $\boldsymbol{\sigma}_{kl}$ associated with each source S_{kl} and perform calculations in the real commutative algebra $\mathcal{A}$ defined by the relations $\boldsymbol{\sigma}_{ij}\boldsymbol{\sigma}_{kl} = \boldsymbol{\sigma}_{kl}\boldsymbol{\sigma}_{ij}$ and $\boldsymbol{\sigma}_{kl}^2 = 3$ for the standard BSM protocol or $\boldsymbol{\sigma}_{kl}^2 = 0$ for the ABSM protocol. Note that real coefficients $\beta_{ij}^{(m,n)} = \mathcal{L}\boldsymbol{\beta}_{ij}^{(m,n)}$ describing the individual success probability of the BSM B_{ij} are obtained via the linear map $\mathcal{L}: \mathcal{A} \to \mathbb{R}$ defined by $\boldsymbol{\sigma}_{kl} \mapsto 1$. Formally, $\mathcal{A}$ may be realized as an even subalgebra of a Clifford algebra with basis $\{\boldsymbol{\sigma}_1, \dots, \boldsymbol{\sigma}_{2N}\}$. Specifically, $\mathcal{A}$ is the subalgebra generated by the bivectors $\boldsymbol{\sigma}_{ij} = \boldsymbol{\sigma}_i\boldsymbol{\sigma}_j$ associated with each source S_{ij}.

The coefficients defining the efficiency of the concatenated link are then given by

$$\beta^{(\vec{v})} = \mathcal{L}\prod_{i=1}^{N-1}\boldsymbol{\beta}_{2i,2i+1}^{(v_i,v_{i+1})}, \tag{17}$$

where the linear map $\mathcal{L}$ is applied to the product taken in $\mathcal{A}$. The relations for $\boldsymbol{\sigma}_{ij}^2$ can be understood as enforcing the correlated probability for simultaneous measurement of oppositely polarized photons from a single source in both channels i and j adjacent to source S_{ij}, where the two distinct relations correspond to the choice of polarization bases used in channels i and j. It should be emphasized that this conditional holds only if both photons of a double pair are detected, leading to the absence of the $\boldsymbol{\sigma}_{ij}$ coefficients in (14)–(16) on the terms associated with the loss of at least one of the photons in the double pair.

A. Efficiency and fidelity of a terminated link

In order to obtain a Bell state with high fidelity when employing probabilistic sources, it is necessary to employ some type of vacuum filtering at the receivers A and B to remove the vacuum component of the state produced by the sources adjacent to the receivers. This could be in the form of a heralded memory or immediate detection of the distributed Bell state. Thus, in the following analyses we assume that the concatenated link is terminated by receivers with vacuum filtering. In the absence of extrinsic noise, employing our simplifying assumption that the outer channels are lossless, the efficiency of a passively concatenated terminated link is

given by

$$\bar{\eta}_{AB} = \sum_{\substack{\vec{v}\in\{0,1,2\}^N \\ v_1,v_N>0}} p^{(\vec{v})}\beta^{(\vec{v})}, \tag{18}$$

where we omit sequences $\vec{v}$ with $v_1 = 0$ or $v_N = 0$.

The Bell state fidelity for the terminated link is

$$F = \frac{\eta_{AB}}{\bar{\eta}_{AB}}, \tag{19}$$

where $\bar{\eta}_{AB}$ appears as the normalization of the state after a successfully terminated BSM chain and η_{AB} is the trace of the projection onto the desired Bell state after the projective measurement of the BSM chain. The latter can be written (see the SM [19])

$$\eta_{AB} = \sum_{\substack{\vec{v}\in\{0,1,2\}^N \\ v_1=v_N=1}} p^{(\vec{v})}\left(\frac{1}{4}\beta^{(\vec{v})} + \frac{3}{4}\left[\frac{2}{3}\right]^{n_2}\hat{\beta}^{(\vec{v})}\right), \tag{20}$$

where n_2 is the number of double pairs $v_i = 2$ in $\vec{v}$ and $\hat{\beta}^{(\vec{v})}$ is the probability of a chain of successful BSMs triggered by exactly one photon from each adjacent source, assuming the corresponding photon numbers $2\vec{v}$ emitted by each source. The coefficient $\hat{\beta}^{(\vec{v})}$ is given by a product of the form (17) except that the Clifford product is replaced by a product of real numbers $\hat{\beta}_{ij}^{(v_i,v_j)}$ obtained from $\boldsymbol{\beta}_{ij}^{(v_i,v_j)}$ by substituting $\boldsymbol{\sigma}_{kl} = 0$ to eliminate all terms where two photons are detected from one source.

A derivation of (20) is given in the SM [19]; however, we note here that the first term can be understood as the minimum contribution to the Bell state fidelity of $\frac{1}{4}$ corresponding to a completely mixed two-photon state shared by A and B. The second term represents an additional contribution if the chain of BSMs is unbroken (i.e., if one photon is detected from each adjacent channel). This additional contribution is reduced by a factor $\frac{2}{3}$ for each double pair, corresponding to the $\frac{1}{3}$ probability of the mixed four-photon term in (3). As a corollary of the result (20), we find that the fidelity of the Bell state produced by a concatenated entanglement swap in the case that all of the secondary photon emissions are lost is

$$F^{(\vec{v})} = \frac{1}{4} + \frac{3}{4}\left(\frac{2}{3}\right)^{n_2}. \tag{21}$$

B. Efficiency and fidelity for repeater chains

For repeater chains supporting multiplexed elementary links, active mode switching allows certain swaps to be performed contingent on the outcome of other BSMs in the chain. In this case, the postmeasurement normalization of the state $\bar{\eta}_{AB}$ does not directly determine the efficiency $\tilde{\eta}_{AB}$ of the link, defined as the number of entangled pairs produced per source mode, which depends on the BSM ordering scheme [7,20]. In this work we restrict our attention to a two-level repeater scheme where all repeater node BSMs are performed simultaneously, independently of the results at neighboring repeater nodes. This assumption is made primarily to simplify the analysis, but it also has the benefit of placing a minimal requirement on the lifetime of the quantum memories employed in the repeaters.

Treating each elementary link connecting sources $S_{i-3,i-2}$ and $S_{i-1,i}$ as a Bernoulli trial with success probability $\bar{\eta}_{i-3,i}$, the average number of source modes (mode pairs for dual-rail qubits) μ_1 needed per elementary link in order to establish a successful BSM in all ℓ elementary links is given by

$$\mu_1 = \frac{1}{\ell} \sum_{i=1}^{\ell} \frac{1}{\bar{\eta}_{4i-3,4i}}. \tag{22}$$

Assuming a two-level scheme, all of the first-level elementary links are discarded if at least one of the repeater node BSMs fails. To determine the success probability of the second level of the link (consisting of all of the repeater node BSMs), we can consider an ensemble of attempts to fully connect a passively concatenated link. Since the sources are all independent, the fraction of attempts in which all of the elementary links succeed is given by $P_1 = \bar{\eta}_{14} \bar{\eta}_{58} \cdots \bar{\eta}_{4\ell-3,4\ell}$. The probability that the second level of the link succeeds is the relative fraction of this subset of attempts for which the full passive link succeeds. The full terminated passive link is connected with probability $\bar{\eta}_{AB}$; hence the probability that the second level of the repeater link succeeds is

$$P_2 = \frac{\bar{\eta}_{AB}}{P_1} = \frac{\bar{\eta}_{AB}}{\bar{\eta}_{14} \bar{\eta}_{58} \cdots \bar{\eta}_{4\ell-3,4\ell}}.$$

Since it takes on average $1/P_2$ attempts for the second level of the link to succeed, the average number of source modes needed to obtain a fully connected chain is given by $\mu_2 = (1/P_2)\mu_1$. Thus, the number of entangled pairs produced per source mode is given by

$$\tilde{\eta}_{AB} = \frac{1}{\mu_2} = \ell \frac{\bar{\eta}_{AB}}{\prod_{i=1}^{\ell} \bar{\eta}_{4i-3,4i} \sum_{j=1}^{\ell} \bar{\eta}_{4j-3,4j}^{-1}}. \tag{23}$$

Assuming that every source node S_{ij} produces pairs at a multiplexed rate weighted by the inverse efficiency $\bar{\eta}_{k-3,k}^{-1}$ of the adjacent elementary link (to avoid bottlenecking the chain), the overall rate at which entangled pairs are produced by the chain is given by

$$R_{AB} = R\tilde{\eta}_{AB}, \tag{24}$$

where R is the average multiplexed pair rate employed by a single source node in the chain. The efficiency $\tilde{\eta}_{AB}$ is the relevant figure of merit for the repeater chain in that it determines the overall entangled pair rate up to the average multiplexed rate R of the source nodes.

Neglecting infidelities introduced by the quantum memories and mode-switching mechanism (i.e., modeling the memories as equivalent to low-loss optical loops which do not affect the state aside from an overall attenuation included in the repeater channel efficiency), the state delivered to A or B by the repeater chain contingent on success of all internal BSMs is identical to the state supplied by passively concatenated links and is thus also given by (9), (19), and (20) [or (18)–(20) for a terminated link]. This follows from the fact that each source is independent and all of the generalized measurement operators associated with different BSMs commute. Thus, the effect of active switching between multiplexed mode pairs available at each repeater node is to more efficiently produce out of an ensemble of equivalent source
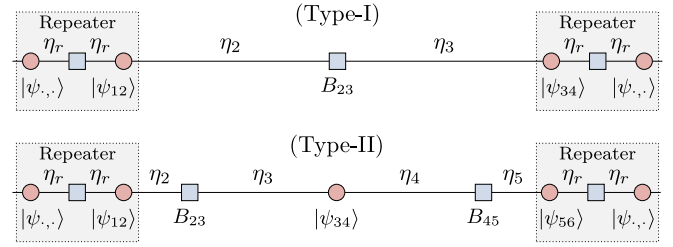

FIG. 2. Two types of elementary links connecting repeater nodes. The type-I link is a typical architecture for a terrestrial quantum network. The type-II link is motivated by the satellite-assisted entanglement distribution, where an entangled pair source distributes pairs $|\psi_{34}\rangle$ to adjacent repeater stations from an orbiting satellite.

states a pair of modes at A and B which have been connected (postmeasurement) by a chain of successful BSMs.

IV. MULTIPHOTON NOISE IN QUANTUM REPEATER CHAINS

In this section we quantify the suppression of multiphoton noise achieved by the ABSM protocol in quantum repeater chains. We consider repeater chains connected by two different types of elementary links shown in Fig. 2, referred to below as type-I and type-II links. The type-I link is a standard entanglement distribution architecture for terrestrial quantum networks (or a satellite uplink) and consists of a single BSM node connecting adjacent repeater nodes. The type-II link is motivated by entanglement distribution via a satellite downlink, where an entangled pair source distributes entangled photons to adjacent repeater stations from an orbiting satellite [21]. In the absence of heralded quantum memories which can efficiently capture relatively broadband photons from a lossy downlink, BSMs B_{23} and B_{45} may be employed to verify transmission of the photon without destroying the entangled state. In general, a type-II link can stand in for any type-I link in a chain; the BSMs fulfill the same role of providing a signal to the repeater nodes that the lossy link has succeeded. As illustrated in Fig. 2, we consider elementary links with general channel efficiencies η_i connecting each source node to the neighboring BSM, with the efficiency of the channels connecting the sources to the repeater node BSMs denoted by η_r.

A. Balanced repeater chains

First, we consider a quantum repeater chain consisting of balanced type-I links with identical channel efficiency $\eta_i \equiv \eta$ adjacent to each BSM and repeater internal efficiency η_r (Fig. 3).

The Bell state fidelity for balanced repeater chains with an arbitrary number of elementary links ℓ is approximated by considering only multipair emission sequences in (18)
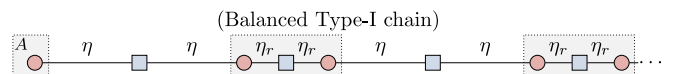

FIG. 3. Repeater chain of balanced type-I elementary links.

with $\vec{\nu}$ containing at most $2\ell + 1$ pairs from $N = 2\ell$ sources. These can be enumerated based on the number of double-pair emissions n_2 in the sequence

$$(2, 1, 1, \ldots, 1), (1, 2, 1, 1, \ldots, 1), \ldots (n_2 = 1),$$

$$(2, 0, 2, 1, 1, \ldots, 1), (1, 2, 0, 2, 1, 1, \ldots, 1), \ldots (n_2 = 2),$$

$$(2, 0, 2, 0, 2, 1, \ldots, 1), (1, 2, 0, 2, 0, 2, 1, \ldots, 1), \ldots (n_2 = 3),$$

and so forth for $n_2 > 3$. Note that there are $2(\ell - n_2 + 1)$ terms for each $n_2 \leqslant \ell$. The ABSM protocol is such that a single source cannot trigger adjacent BSMs; hence it completely eliminates all errors with $n_2 > 2$. Since the number of error terms with $n_2 = 1$ and 2 grows linearly with the length of the chain ℓ while the remaining errors with $n_2 > 2$ grow quadratically in ℓ, the ABSM protocol completely suppresses the dominant quadratic growth of multiphoton errors for long repeater chains.

To quantify this we use the expressions of Sec. III to derive the Bell state fidelity for a balanced repeater chain of arbitrary length. Remarkably, using the Clifford product, the sums in (18)–(20) can be evaluated in closed form, yielding a compact expression for the fidelity

$$F = \frac{1 + p\left(\varepsilon_+ + \frac{11+\sigma}{5+\sigma}\varepsilon_1\right) + O(p^2)}{1 + 4p(\varepsilon_1 + \varepsilon_1' + \varepsilon_+ + \varepsilon_+') + O(p^2)}, \quad (25)$$

where $p \equiv p_{ij}$ is the source emission probability, the terms ε_1' and ε_1 give the contribution from $n_2 = 1$ errors

$$\varepsilon_1' = (1 - \eta), \quad (26)$$

$$\varepsilon_1 = \frac{\ell - 1}{2}(5 + \sigma)(1 - \eta)(1 - \eta_r), \quad (27)$$

and ε_+' and ε_+ represent the remaining sum for $n_2 > 1$, taking the value $\varepsilon_+ = \varepsilon_+' = 0$ for $\ell = 1$ and

$$\varepsilon_+' = \frac{1}{4}(1 + \sigma)[1 + \sigma(\ell - 2)](1 - \eta), \quad (28)$$

$$\varepsilon_+ = \frac{\ell - 2}{4}(1 + \sigma)^2[2 + \sigma(\ell - 3)](1 - \eta)(1 - \eta_r) \quad (29)$$

for $\ell > 1$, where $\sigma = \sigma_{ij}^2/3$ depends on the BSM protocol. The coefficient σ completely captures the noise suppression provided by the ABSM protocol with $\sigma = 1$ for the nonalternating BSM protocol and $\sigma = 0$ for the ABSM protocol. The terms ε_1' and ε_+' represent the contribution from boundary sequences with multipair emissions $\nu_1 = 2$ or $\nu_N = 2$.

The last term (29) quantifies the dominant ℓ^2 growth of multiphoton errors in (25) when $\sigma = 1$; however, this quadratic term vanishes when employing the ABSM protocol ($\sigma = 0$). Note that the fidelity is essentially independent of the channel efficiency η for $\eta \ll 1$ since we can use the approximation $(1 - \eta) \simeq 1$. The Bell state fidelity for the balanced chain thus depends only on the repeater efficiency η_r, the source emission probability p, and the number of elementary links ℓ. The dependence of the Bell state fidelity on the length of the chain is shown in Fig. 4 for repeaters with $\eta_r = 0.9$.

Note the significant improvement in fidelity provided by the ABSM protocol as the length of the chain increases. The impact of this on repeater chains employing probabilistic sources can be translated into a gain G in efficiency for each
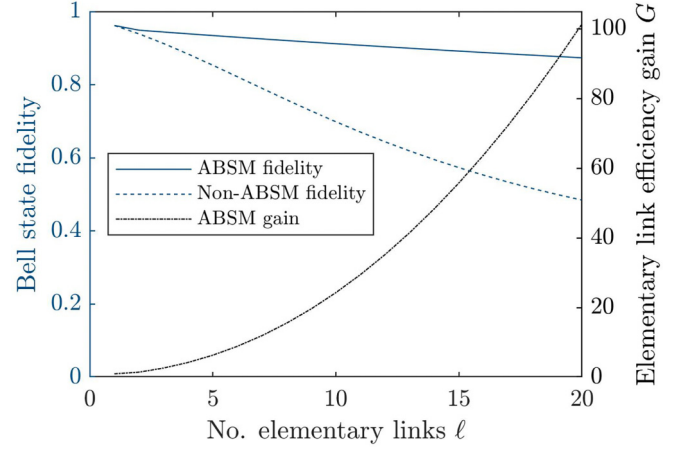

FIG. 4. Bell state fidelity from the leading-order approximation (25) for repeater chains using probabilistic sources with emission probability $p = 0.01$ and repeater internal efficiency $\eta_r = 0.9$. The axis on the right shows the gain in elementary link efficiency (30) and (31) provided by the ABSM protocol if the emission probabilities are adjusted to achieve a Bell state fidelity $F = 0.9$ with $\eta_r = 0.9$.

elementary link subject to a fixed fidelity F by inverting (25) for the allowed emission probability

$$p(F; \sigma) = \frac{1 - F}{4F(\varepsilon_1 + \varepsilon_1' + \varepsilon_+ + \varepsilon_+') - \varepsilon_+ - \frac{11+\sigma}{5+\sigma}\varepsilon_1}. \quad (30)$$

The elementary link efficiency depends on the square of the emission probability p, and so the gain is given by

$$G = \frac{p(F; \sigma = 0)^2}{p(F; \sigma = 1)^2}. \quad (31)$$

The result is shown in Fig. 4 for chains with $\eta_r = 0.9$, assuming fixed fidelity $F = 0.9$. From (30) and (31) we see that the gain grows quadratically with the length of the chain, reaching a 20-fold increase for a chain with $\ell = 10$ elementary links. This quadratic growth can again be understood in correspondence to our earlier observation of the suppression of errors with $n_2 > 2$.

Employing the two-level repeater model presented in Sec. III, the overall link efficiency for a chain with total combined channel loss η_c divided into ℓ elementary links is

$$\tilde{\eta}_{AB} = \frac{\bar{\eta}_{AB}}{\bar{\eta}_{EL}^{\ell-1}} = p^2\eta^2\frac{\eta_r^{2(\ell-1)}}{2^{2\ell-1}} + O(p^3), \quad (32)$$

where $\eta = \eta_c^{1/2\ell}\eta_d$, η_d is the efficiency of the detectors used for the linear optical BSMs at the center of the elementary links, and

$$\bar{\eta}_{EL} \equiv \bar{\eta}_{14} = \bar{\eta}_{58} = \cdots = \bar{\eta}_{4\ell-3,4\ell} = p^2\eta^2 + O(p^3) \quad (33)$$

is the elementary link efficiency for the balanced chain (including double-pair errors). To lowest order in the pair probability p, the result is the elementary link efficiency $\bar{\eta}_{EL}$ reduced by the factor $\eta_r^{2(\ell-1)}/2^{2\ell-1}$ arising from the repeater efficiency and 50% success probability of the $2\ell - 1$ linear optical BSMs (here η_r should be understood to include the
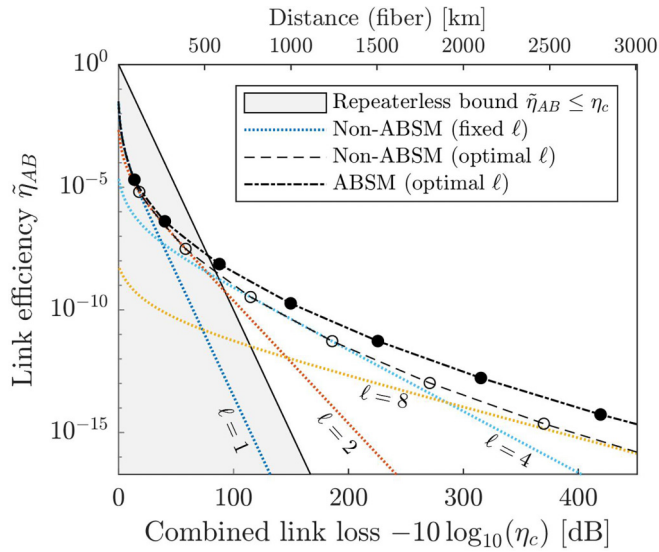
FIG. 5. Link efficiency as a function of total link loss for a repeater chain using PDC sources with pair probability configured to yield a Bell state fidelity $F = 0.9$ with $\eta_r = \eta_d = 0.9$ based on (32) and (30). The dotted curves show the efficiency without the ABSM protocol for $\ell = 1, 2, 4$, and 8. The dashed curves show the maximum efficiency optimizing the number of links ℓ with and without the ABSM protocol. The markers show where the optimal number of links increases. The shaded region shows the repeaterless bound $\tilde{\eta}_{AB} \leqslant \eta_c$ for perfect deterministic sources.
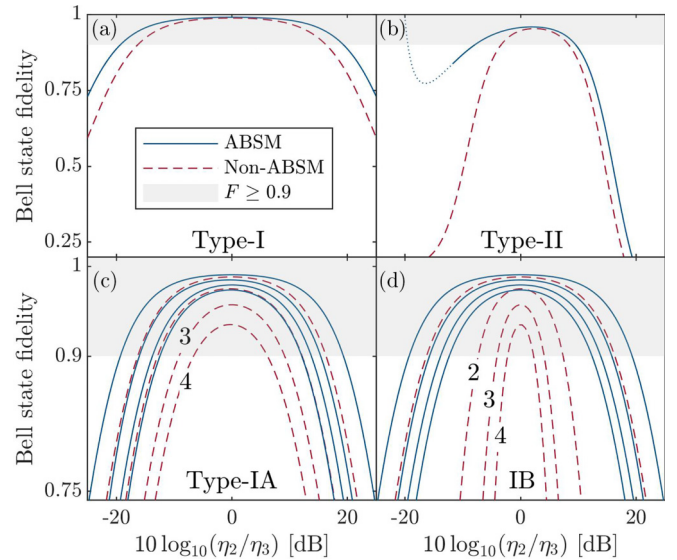

FIG. 6. (a) and (b) Bell state fidelity for a single elementary link (cf. Fig. 2) with imbalanced channels dividing 40 dB combined loss with pair probability $p = 0.01$. (c) and (d) Fidelity for the type-I repeater chains shown in Fig. 7 with $\ell = 1, 2, 3$, and 4 elementary links (from top to bottom). The type-II link assumes a symmetric imbalance $\eta_2 = \eta_5$ and $\eta_3 = \eta_4$; the dotted curve denotes the domain where three-pair emissions (neglected in this analysis) become a dominant source of noise. Results are based on direct evaluation of (18)–(20).

detection efficiency of the repeater node BSM). Figure 5 shows the link efficiency as a function of the total combined loss η_c, translated into a terrestrial link distance by assuming a fiber attenuation of 0.15 dB/km.

Note that even without the ABSM protocol, the repeater chain with PNR BSMs can outperform the repeaterless bound $\tilde{\eta}_{AB} \leqslant \eta_c$ for distribution of entangled photon pairs using a perfect deterministic pair source. More precisely, assuming repeaters with internal efficiency $\eta_r = 0.9$, the repeater architecture analyzed here first surpasses this ideal repeaterless link at fidelity $F = 0.9$ with an optimal number $\ell = 3$ elementary links dividing a combined loss of 83 dB. However, in order to achieve a rate of 10^5 pairs/s at this range requires a multiplexed repetition rate approximately 10^{13} Hz from each source. This result is very similar the multiplexed rate of 3×10^{13} Hz found to surpass an ideal repeaterless quantum key distribution bound at a rate of approximately 10^5 secret key bits/s in a similar PDC repeater architecture studied in [10]. In that work an ideal repeaterless bound was also found to be first surpassed using three elementary links to divide a combined loss of approximately 90 dB assuming sources with 10^4 frequency modes and 100 spatial modes operated at a repetition rate of 30 MHz.

The upper envelope for the link efficiency, optimizing the number of links ℓ for a given total link loss, is shown in Fig. 5 for both the standard protocol and the ABSM protocol. As the link efficiency $\tilde{\eta}_{AB}$ is proportional to the elementary link efficiency $\bar{\eta}_{EL}$ and determines the entangled pair rate up to the multiplexed rate R of each source, the gain in the entangled pair distribution rate provided by the ABSM protocol is in direct correspondence to the elementary link gain shown in

Fig. 4 and reaches a factor of 10 for chains with $\ell = 6$ elementary links.

B. Noise suppression for elementary links with imbalanced losses

The results of the preceding section show that using PDC-based repeaters, very high multiplexed source rates are required to achieve appreciable entangled pair rates at $100 + $ dB combined link loss. Thus, even with repeaters, long-distance links based on PDC sources demand a more efficient conversion from combined link loss to link distance than is provided by the approximately 0.15 dB/km from fiber transmission loss. Satellite-assisted links governed by free-space diffraction loss can make more effective use of the allowable total link loss to achieve longer range links; however, the architecture of satellite-assisted links restricts the location of BSM nodes leading to dynamic imbalanced channels which can be detrimental to PDC-based links with multiphoton noise.

Motivated by this problem, we analyze the additional suppression of multiphoton noise provided by the ABSM protocol in chains with imbalanced channel losses. To quantify this, we first consider the reduction in fidelity caused by imbalanced losses which are not compensated by a corresponding suppression of single-pair emissions; an analysis of the gain provided by the protocol if the imbalanced losses are compensated is given in Sec. V. Figure 6 shows the dependence of the fidelity on channel losses for elementary links with 40 dB combined loss, assuming the source emission probabilities are all fixed at $p_{ij} = 0.01$ and the multipair
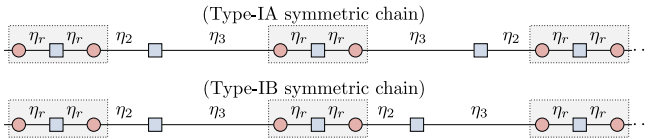
FIG. 7. Repeater chains of imbalanced type-I elementary links with special symmetries which demonstrate the nonlocality of multiphoton noise in extended repeater chains.

emissions are governed by (2). An efficiency $\eta_r = 0.9$ is assumed for all channels internal to the quantum repeaters.

Figure 6(a) shows that the type-I link fidelity is symmetric in the link imbalance and the ABSM protocol supports an additional 3 dB difference in channel losses at 90% state fidelity. Figure 6(b) shows the type-II link fidelity for symmetric imbalances $\eta_2 = \eta_5$ and $\eta_3 = \eta_4$ (cf. Fig. 2). The ABSM protocol significantly suppresses multiphoton noise for type-II links such that both BSMs are located closer to the central source. In this case, the ABSM fidelity remains above 74%, supporting an additional 5 dB imbalance at 90% state fidelity. On the other hand, if both BSMs are located closer to the repeater nodes, as in the satellite downlink architecture described above, the ABSM protocol only supports an additional 1–2 dB difference in channel losses at 90% state fidelity.

As the length of the repeater chain grows, the reduction in fidelity is compounded as shown in the preceding section for balanced links (25)–(29). This reduction is even more severe in the presence of imbalanced channels; however, Figs. 6(c) and 6(d) show that the ABSM protocol is more resilient to this reduction in fidelity for longer chains of type-I links.

Figure 6 also shows that the severity of multiphoton noise from chains of imbalanced links can depend significantly on the direction in which each elementary link is imbalanced. The dependence of the fidelity on the link imbalance is shown for chains of imbalanced type-I links with two special symmetry types, labeled type-IA and type-IB (Fig. 7). The type-IA chain is defined with the links imbalanced in alternating directions, so $\eta_2 \leftrightarrow \eta_3$ are exchanged for adjacent elementary links. The type-IB chain is defined such that all of the links are imbalanced in the same direction (and by the same amount). Note that the Bell state fidelity degrades much more quickly in the type-IB chain using the standard BSM protocol. This behavior shows that multiphoton noise in a quantum repeater chain cannot be considered purely locally, i.e., noise can propagate down the chain.

To understand this phenomenon, we must consider the dominant source of multiphoton noise in each chain. In the type-IB chain, the dominant noise in (18) is given by double pairs separated by a single intermediate source. These can be connected through successful BSMs by subsequences $\vec{v}$ of the form $(2, 0, 2, 0, \dots, 2)$ consisting of only $N + 1$ photon pair emissions from N sources. Conversely, the dominant source of multiphoton noise in the type-IA chain comes from double pairs separated by an even number of intermediate sources, e.g., $(2,2)$ or $(2,1,1,2)$, which require at least $N + 2$ pair emissions from N sources and are thus not as prominent. In this way, we see that the repeater nodes do not insulate multiphoton errors from neighboring links, i.e., the final Bell

state fidelity cannot generally be determined by combining an independent reduction in fidelity from each elementary link.

Indeed, this lack of independence of the multipair noise is precisely the property that the ABSM protocol takes advantage of, since multipair events are suppressed based on their correlation to multipair events in neighboring links. In doing so, the ABSM protocol can be seen to block the propagation of these errors. Specifically, the ABSM protocol yields essentially the same fidelity for both type-IA and type-IB chains. This can be understood by the observation that the ABSM protocol does not allow a BSM chain to be connected by emission sequences of the form (0,2,0), which produce the dominant error in the type-IB chain.

V. MULTIPHOTON NOISE IN TYPE-II ELEMENTARY LINKS

In this section we consider an application of the ABSM protocol to elementary links consisting of two simultaneous entanglement swaps (type-II links). This type of architecture is motivated by a satellite downlink and avoids many engineering challenges associated with establishing a synchronized low-loss optical uplink through earth's atmosphere. The idea of the type-II link is to use an entanglement swap with a high-rate probabilistic photon source as a quantum nondemolition (QND) measurement of the presence of another photonic entangled state before or after a lossy entanglement distribution link. For example, in the absence of heralded quantum memories which can efficiently capture relatively broadband photons from a lossy downlink, one can instead position a PDC source in a ground station receiving a satellite downlink to verify transmission of a photon using a local BSM.

One of the drawbacks of using a PDC source in this manner is that if a BSM is not centrally located between two PDC sources, one source can dominate the BSM with double pairs relative to the two-photon coincidences with one photon from each side. This is detrimental to the efficiency of the link, since it requires that the link be artificially balanced by reducing the emission probability of the source close to the BSM to suppress double pairs. In a double entanglement swap the ABSM protocol can identify some of the double-pair errors potentially allowing for a higher emission probability. Double pairs can be further suppressed by combining the ABSM protocol with a cascaded entangled pair source as described in [11], which employs a high-efficiency BSM with PNR to herald the production of a single entangled pair. Before proceeding to an analysis of entanglement distribution with cascaded PDC sources, we first demonstrate the principle by quantifying the gain afforded by the ABSM protocol for a terminated elementary link consisting of two passively concatenated entanglement swapping links with three independent sources (Fig. 8).

A. Maximum efficiency for double entanglement swap with probabilistic sources and imbalanced links

In the following analysis, we assume that the double entanglement swapping link is passively concatenated (i.e., both BSMs must succeed simultaneously for a successful
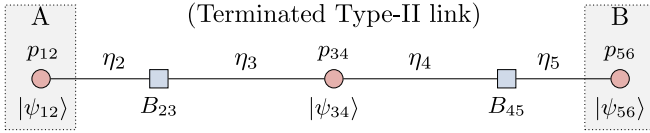
FIG. 8. Terminated type-II link motivated by the satellite-assisted entanglement distribution. The efficiency of the link with PDC sources and imbalanced losses η_i depends on the maximum allowed pair probabilities p_{12}, p_{34}, and p_{56} subject to a constraint on the minimum Bell state fidelity.

entanglement distribution). Following the model of a terminated link presented in Sec. III, the probability of a fourfold coincidence with opposite polarizations in each BSM and at least one photon sent to A and B during a single use of the link takes the form

$$\bar{\eta}_{AB} = \sum_{\substack{i,j,k=0 \\ i,j>0}}^{2} p_{12}^{(i)} p_{34}^{(j)} p_{56}^{(k)} \beta^{(i,j,k)}, \quad (34)$$

where the coefficient $\beta^{(l,m,n)}$ describes the probability of a fourfold coincidence associated with an l-pair emission from source S_{12}, m-pair emission from source S_{34}, and n-pair emission from source S_{56}. We neglect events with more than four total photon pairs produced by the three sources.

The primary coefficient is the $(1,1,1)$ coefficient describing the probability of two simultaneously successful BSMs given a single-pair emission from each source

$$\beta^{(1,1,1)} = \tfrac{1}{4}\eta_2\eta_3\eta_4\eta_5. \quad (35)$$

The leading-order error coefficients are then calculated explicitly from Clifford products of (13)–(15) as

$$\hat{\beta}^{(1,2,1)} = \eta_2\eta_3\eta_4\eta_5(1-\eta_3)(1-\eta_4), \quad (36)$$

$$\beta^{(1,2,1)} = \hat{\beta}^{(1,2,1)} + \frac{\sigma}{3}\eta_3^2\eta_4^2(1-\eta_2)(1-\eta_5)$$
$$+ \frac{1}{3}\eta_2\eta_3\eta_4^2(1-\eta_3)(1-\eta_5) + \frac{1}{3}\eta_3^2\eta_4\eta_5$$
$$\times (1-\eta_2)(1-\eta_4), \quad (37)$$

$$\beta^{(2,1,1)} = \frac{1}{2}\eta_2\eta_3\eta_4\eta_5(1-\eta_2) + \frac{1}{6}\eta_2^2\eta_4\eta_5(1-\eta_3), \quad (38)$$

$$\beta^{(2,0,2)} = \frac{1}{9}\eta_2^2\eta_5^2, \quad (39)$$

with the $(1,1,2)$ coefficient related to the $(2,1,1)$ coefficient via the index substitution $2 \leftrightarrow 5$ and $3 \leftrightarrow 4$. The parameter $\sigma = \sigma_{34}^2/3$ again captures the suppression of double-pair emission noise achieved using an alternating basis in the BSMs, with $\sigma = 0$ for the ABSM protocol and $\sigma = 1$ using nonalternating BSMs. Note that this suppression is most significant when link imbalances are such that $\eta_3^2\eta_4^2$ is the dominant term. The last two coefficients above are unaffected by the protocol since they do not include events where the source adjacent to both BSMs produces a double pair; however, as discussed at the end of the section, these noise events can be suppressed by QND measurements with PNR at the receivers A and B since double-pair states are produced at an outer node.

For the double-swap link, the Bell state fidelity is

$$F = p_{12}p_{56}\frac{p_{34}\beta^{(1,1,1)} + p_{34}^{(2)}\left[\frac{1}{4}\beta^{(1,2,1)} + \frac{1}{2}\hat{\beta}^{(1,2,1)}\right]}{\bar{\eta}_{AB}}. \quad (40)$$

To obtain analytical results, we will approximate the fidelity F by calculating $\bar{\eta}_{AB}$ using only the leading-order error coefficients given above.

Assuming the multipair emissions are governed by (2), we approximate the relation of single-pair to double-pair emissions as

$$p_{ij}^{(2)} \simeq \tfrac{3}{4}p_{ij}^2. \quad (41)$$

The impact of multipair emission noise for fixed link losses η_i is determined by considering the maximum efficiency subject to a fixed infidelity Δf,

$$\hat{\eta}_{AB}(\Delta f) = \max_{p_{12},p_{34},p_{56}} \left\{\eta_{AB} : F \geqslant 1 - \Delta f, \; p_{ij} \leqslant \tfrac{8}{27}\right\}, \quad (42)$$

where the maximum is taken over all emission probabilities satisfying $p_{ij} \leqslant \frac{8}{27} \simeq 0.3$ in accord with the maximum allowable single-pair probability in (2).

In order to analyze the maximum efficiency we use the method of Lagrange to solve the constrained optimization under the assumption that the optimum $\hat{\eta}_{AB}(\Delta f)$ is obtained on the boundary $F = 1 - \Delta f$ with $p_{ij} < \frac{8}{27}$, conditions that generally hold provided all channels have losses $\eta_i < 1$ and Δf is sufficiently small. The Lagrangian constraint leads to a relation defining the relative pair probabilities which maximize the efficiency η_{AB} for fixed fidelity (see the SM [19])

$$p_{12}b_{12} = p_{34}b_{34}w(b) = p_{56}b_{56} \equiv p, \quad (43)$$

where the weights are given by

$$b_{12} = \beta^{(2,1,1)}, \quad b_{56} = \beta^{(1,1,2)}, \quad (44)$$

$$b_{34} = \tfrac{3}{4}\beta^{(1,2,1)} - \tfrac{1}{2}\hat{\beta}^{(1,2,1)} \quad (45)$$

and the central source emission probability has an additional weight $w(b) = 2/(1 + \sqrt{1 + 6b})$ associated with balancing the $\beta^{(2,0,2)}$ noise determined by the parameter

$$b = \frac{b_{34}\beta^{(2,0,2)}}{b_{12}b_{56}}. \quad (46)$$

The latter satisfies $\sigma/36 \leqslant b \leqslant 1$ and increases as the BSMs move farther from the central source towards the outer sources.

Noting that F is a differentiable function of the parameter p with nonvanishing derivative at $p = 0$, the linear approximation to p determining the optimal probabilities p_{ij} can be evaluated near $\Delta f = 0$,

$$p = \frac{16\beta^{(1,1,1)}}{36 + 27bw(b)}\Delta f + O((\Delta f)^2), \quad (47)$$

yielding the maximum efficiency with infidelity Δf,

$$\hat{\eta}_{AB} = \frac{16^3[\beta^{(1,1,1)}]^4}{b_{12}b_{34}b_{56}w(b)[36 + 27bw(b)]^3}(\Delta f)^3 + O((\Delta f)^4). \quad (48)$$

This expression has been derived based on the assumption that the multiphoton error is dominated by the leading-order

coefficients (36)–(39). This generally holds true for the non-ABSM protocol ($\sigma = 1$); however, for severely imbalanced links with $\eta_2 \ll \eta_3$ and $\eta_5 \ll \eta_4$ the ABSM protocol ($\sigma = 0$) yields nearly complete suppression of the dominant $\beta^{(1,2,1)}$ error coefficient. Once this suppression approaches the pair generation probability p_{34}, the error can become dominated by three-pair emissions associated with the $(1,3,1)$ error and the $O((\Delta f)^4)$ term must be calculated including error coefficients $\beta^{(i,j,k)}$ for higher-order terms. To estimate the domain where three-pair emissions become relevant, we rewrite the error coefficient $\beta^{(1,2,1)}$ in the form

$$\beta^{(1,2,1)} = \tfrac{1}{3}\eta_3^2\eta_4^2(1 - \eta_2)(1 - \eta_5)(\sigma + 3\lambda_{23}\lambda_{54} + \lambda_{23} + \lambda_{54}),$$

$$(49)$$

where the parameters

$$\lambda_{ij} = \frac{\eta_i(1 - \eta_j)}{\eta_j(1 - \eta_i)} \tag{50}$$

characterize the difference in channel losses adjacent to each BSM. The error suppression approaches the pair generation probability for

$$3\lambda_{23}\lambda_{54} + \lambda_{23} + \lambda_{54} \lesssim 0.1, \tag{51}$$

giving a general criterion whereupon three-pair emissions become a relevant source of error.

B. Efficiency penalty and ABSM gain for imbalanced links with probabilistic sources

In order to gain insight into the main result (48) from the preceding section, we factor the expression in the form

$$\hat{\eta}_{AB} = \pi_0 \beta^{(1,1,1)} \hat{\pi}(\eta_2, \eta_3, \eta_4, \eta_5) + O((\Delta f)^4), \tag{52}$$

where $\beta^{(1,1,1)}$ represents the efficiency of the link with deterministic entangled pair sources and π_0 represents the combined source efficiency $p_{12}p_{34}p_{56}$ using probabilistic sources in the limit of balanced low-efficiency links $\eta_2 = \eta_3 = \eta_4 = \eta_5 \ll 1$. The remaining factor $\hat{\pi}$ captures both the balancing loss associated with a reduction in source efficiency required to compensate for imbalanced channels and the gain from PNR in the BSM detectors which discards multiphoton events when at least three photons are detected.

Using the results from the preceding section, the combined source efficiency in the limit of balanced lossy channels is given by

$$\pi_0 = \begin{cases} 0.0027(\Delta f)^3, & \sigma = 1 \\ 0.0037(\Delta f)^3, & \sigma = 0 \end{cases} \tag{53}$$

for type II. For comparison, the combined source efficiency π_0 for a balanced type-I link can be obtained from (30) by setting $\ell = 1$ and is given to leading order in Δf as

$$\pi_0 = 0.0625(\Delta f)^2. \tag{54}$$

Thus, even with balanced losses the type-II link suffers an additional factor of $0.04\Delta f$ efficiency reduction relative to the single-swap type-I link.

The efficiency is further reduced in the presence of imbalanced losses between the sources and BSMs. The additional loss factor $\hat{\pi}$ is shown in Fig. 9 for a link with 40 dB combined
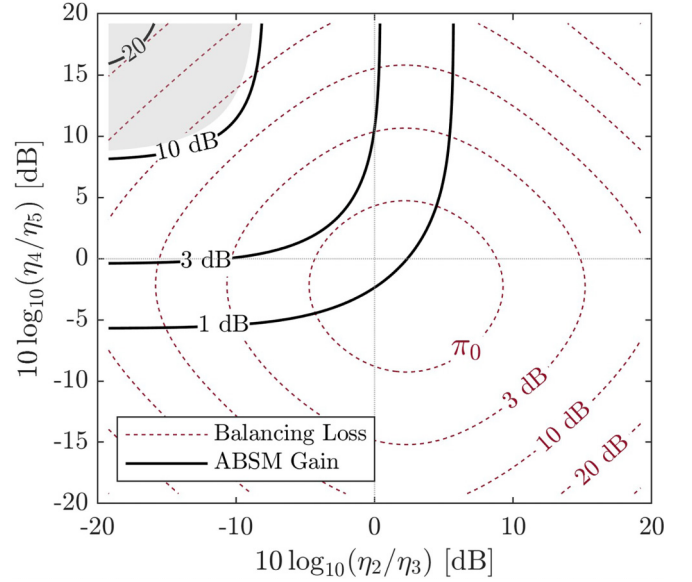

FIG. 9. Gain in link efficiency from the ABSM protocol for a type-II link, shown in comparison to the balancing loss $-10\log_{10}(\hat{\pi})$ for the standard BSM protocol ($\sigma = 1$) based on the leading-order approximation (48)–(52). A maximum value of $\hat{\pi} = 1.86$ is attained with the BSMs slightly biased towards the outer sources due to the higher Bell state fidelity of the $(1,2,1)$ error. The shaded region estimates the domain where three-pair emissions (neglected in this analysis) must be taken into account due to the strong suppression of double-pair errors described by (51).

losses $\eta_2\eta_3 = \eta_4\eta_5 = 0.01$. The result is an additional 20–30 dB loss for the fully imbalanced link, i.e., the compensation required to balance the link reduces the combined source efficiency by a factor on the order of the channel efficiency ratios η_2/η_3 and η_4/η_5.

To understand the gain in source efficiency provided by the ABSM protocol, we return to the expression (48) and find that the gain can be written

$$G = \frac{bw(b)[36 + 27w(b)]^3|_{\sigma=1}}{bw(b)[36 + 27w(b)]^3|_{\sigma=0}}\left(1 + \frac{1}{\lambda_{23} + \lambda_{54} + \lambda_{23}\lambda_{54}}\right),$$

$$(55)$$

which depends only on the channel efficiency ratios λ_{ij}. This dependence is made more explicit by expressing the parameter b in the form

$$b = \frac{\sigma + \lambda_{23} + \lambda_{54} + \lambda_{23}\lambda_{54}}{9 + 3\lambda_{23} + 3\lambda_{54} + \lambda_{23}\lambda_{54}}. \tag{56}$$

The result is shown in Fig. 9 for the same link with 40 dB combined channel loss. As expected, the ABSM protocol significantly mitigates the balancing loss when both BSMs are biased towards the central source $\lambda_{23}, \lambda_{54} < 1$.

If both links are balanced, the ABSM protocol yields a 1.4 dB gain, with an increase to 3 dB if only one BSM is closer to the central source. The general gain predicted by (48) can

be summarized by the limiting cases

$$
G \simeq \begin{cases}
1.1\left(1 + \frac{1}{2\lambda_{23}}\right), & \lambda_{23} = \lambda_{54} \ll 1 \\
1, & \lambda_{23} = \lambda_{54} \gg 1 \\
2.1, & \lambda_{23} \ll \lambda_{54} = 1 \\
1.4, & \lambda_{23} = \lambda_{54} = 1 \\
1, & \lambda_{23} \gg \lambda_{54} = 1.
\end{cases} \tag{57}
$$

Unfortunately, the ABSM protocol does not yield any gain for the type of imbalance inherent in the satellite-assisted downlink ($\lambda_{23}, \lambda_{54} \gg 1$). This is to be expected, since the primary double-pair errors in this case arise from double pairs produced by the outer sources which go unchecked by the ABSM protocol. However, by employing cascaded PDC sources in place of S_{12} and S_{56}, which themselves perform an internal BSM, the ABSM protocol can be used to reduce the double-pair errors associated with the imbalance $\lambda_{23}, \lambda_{54} \gg 1$.

The type-II link with cascaded PDC sources is analyzed in the next section. Before proceeding to that analysis, we note that another technique for achieving a type-II link commensurate with a type-I link is to equip the receivers at A and B with QND measurements with PNR to discard multiphoton events from sources S_{12} and S_{56}, respectively. The maximum efficiency $\hat{\eta}_{AB}$ then increases with the higher emission probabilities p_{12} and p_{56} afforded by the ability to identify and discard double-pair emission events from the end nodes. The effect of receiver PNR is to reduce $\beta^{(2,1,1)}$, $\beta^{(1,1,2)}$, and $\beta^{(2,0,2)}$ (describing the probability of a nominally successful double swap given the corresponding photon numbers from each source) by a corresponding constant factor. Specifically, $\beta^{(2,1,1)}$ and $\beta^{(1,1,2)}$ are reduced by the factor $1 - \alpha$, where α represents the proportion of two-photon emission events from the adjacent source which are identified by the receiver, while $\beta^{(2,0,2)}$ is reduced by $(1 - \alpha)^2$. The parameter b defined by (46) is left invariant and hence the maximum efficiency (48) is simply increased by $(1 - \alpha)^{-2}$ independently of channel losses η_i and BSM protocol σ.

C. ABSM gain for a type-II elementary link with cascaded PDC sources

In the preceding section it was shown that the ABSM protocol provides the most significant gain for double-swap links where the BSMs are close to the central source. As noted above, this is contrary to the type of imbalance inherent in the type-II elementary link motivated by a satellite downlink. Nevertheless, we now show that by introducing an additional BSM at each end of the link one can take advantage of the ABSM protocol to enable a type-II downlink. The basic idea is to employ a multiplexed cascaded PDC source at both ends of the link to suppress double-pair emissions from the end nodes (Fig. 10). The principle of a cascaded source is to use an active optical switch to route entangled pairs produced by a bank of PDC sources into a single output based on a successful BSM performed internally within the multiplexed source [11]. This can be modeled as an inverted repeater architecture which is equivalent to the type-II elementary link shown in Fig. 2 except that the repeater nodes now represent cascaded sources, with the repeater node swaps performed *before* the BSMs interfering with the downlink.
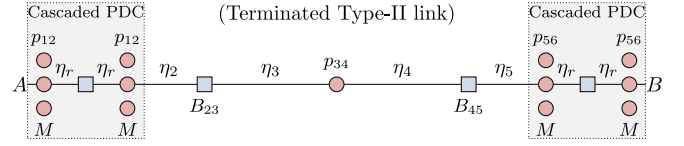

FIG. 10. Terminated type-II link with cascaded sources motivated by the satellite-assisted entanglement distribution. To maximize the utilization of photons from a satellite downlink, multiplexed cascaded PDC sources first use an internal BSM to herald production of an entangled pair before interfering with a photon from a satellite downlink.

To model the efficiency of this architecture, we assume that the cascaded sources S_{12} and S_{56} are configured such that all internal sources have the same emission probability p_{12} and p_{56}, respectively. Following the procedure of the previous section, we find the optimization follows an essentially equivalent mathematical form, with the optimal probabilities satisfying the same relation (43) with a redefinition of the weights given by (see the SM [19])

$$
b_{12} = \frac{1}{2}\left(\beta^{(21111)} + \frac{3}{4}\beta^{(12111)} - \frac{1}{2}\hat{\beta}^{(12111)}\right), \tag{58}
$$

$$
b_{56} = \frac{1}{2}\left(\beta^{(11112)} + \frac{3}{4}\beta^{(11121)} - \frac{1}{2}\hat{\beta}^{(11121)}\right), \tag{59}
$$

$$
b_{34} = \frac{3}{4}\left(\beta^{(11211)} - \frac{2}{3}\hat{\beta}^{(11211)} + \beta^{(20211)}\right. \tag{60}
$$

$$
\left. + \beta^{(11202)} + \frac{3}{4}\beta^{(20202)}\right) \tag{61}
$$

and

$$
b = \frac{9}{16}\frac{b_{34}\beta^{(12021)}}{b_{12}b_{56}} \tag{62}
$$

determining the balancing of the multiphoton noise. The parameter p defined by (43) takes the modified form

$$
p = \frac{8\beta^{(11111)}}{30 + 15bw(b)}\Delta f + O((\Delta f)^2). \tag{63}
$$

The resulting maximum efficiency can be factored in the form of (52) as

$$
\hat{\eta}_{AB}(\Delta f) = \pi_0 \frac{1}{4}\eta_2\eta_3\eta_4\eta_5\hat{\pi}(\eta_2, \eta_3, \eta_4, \eta_5) + O((\Delta f)^6). \tag{64}
$$

The domain requiring consideration of three-pair errors is again given by (51), arising from similar limits on the suppression of the $\beta^{(11211)}$, $\beta^{(20211)}$, and $\beta^{(11202)}$ error coefficients.

The source efficiency π_0 in the low-efficiency limit is

$$
\pi_0 = \frac{M^2\eta_r^4}{(1 - \eta_r)^4}(\Delta f)^5 \times \begin{cases} 3 \times 10^{-8}, & \sigma = 1 \\ 2 \times 10^{-7}, & \sigma = 0, \end{cases} \tag{65}
$$

where M is the number of pairs of PDC sources multiplexed in each cascaded source and η_r is the internal efficiency. To simplify the analysis we assume M is not too large relative to the efficiency of the cascaded source internal swap $M \ll 32/(\eta_r\Delta f)^2$. The benefit of introducing the cascaded sources is to give some engineering control over the type-II link efficiency, obtained via the multiplexing factor M and internal
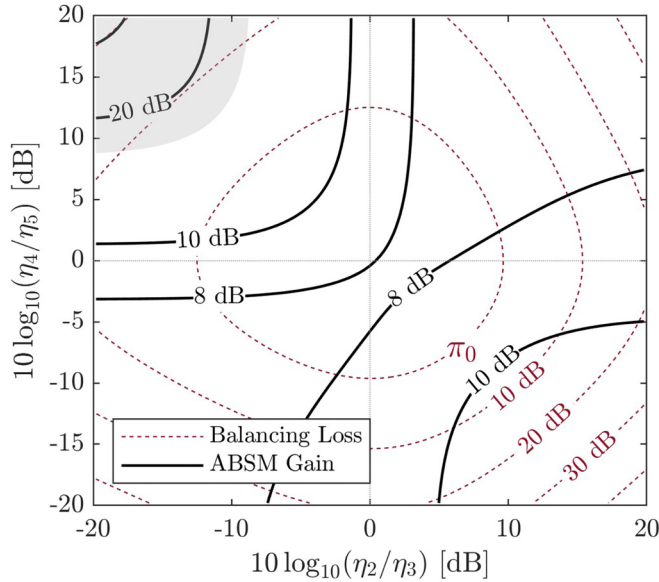
FIG. 11. Gain in link efficiency $\hat{\eta}_{AB}$ from the ABSM protocol for a type-II link with cascaded PDC sources based on (58)–(64). The result is shown against the balancing loss $-10\log_{10}(\hat{\pi})$ for the non-ABSM protocol ($\sigma = 1$). The center of the plot corresponds to balanced losses between the sources and the BSMs where a maximum value of $\hat{\pi} = 6.3$ is attained. The shaded region estimates the domain where three-pair emissions should be taken into account as in Fig. 9.

efficiency η_r of the cascaded source. It should be observed that a high degree of multiplexing is required to overcome the $10^{-5}(\Delta f)^2$ efficiency reduction relative to the passive double-swap link (53) or the $4 \times 10^{-6}(\Delta f)^3$ reduction relative to the type-I single-swap link. As the multiplexing factor approaches the internal swap efficiency $M \sim 32/(\eta_r \Delta f)^2$, the cascaded source becomes a nearly deterministic source and a more detailed analysis is required [11].

For a type-II link with the BSMs located close to the cascaded sources, the balancing loss must also be taken into account and is shown in Fig. 11 for the same 40 dB combined loss as in Fig. 9. Figure 11 also shows the gain provided by the ABSM protocol, in direct correspondence to the type-II link shown in Fig. 9. The presence of the repeater nodes (i.e., cascaded sources) at the ends of the type-II link allows the ABSM protocol to be employed to discard multiphoton events in the two central BSMs. This compensates for the balancing loss with up to 12 dB gain for BSMs close to the cascaded sources.

As an example, for a fully imbalanced type-II link with 40 dB combined loss targeting a 95% Bell state fidelity, the passive double-swap using PDC sources analyzed in the previous section yields a 48 dB efficiency reduction relative to a balanced type-I link with the same combined loss. With a multiplexing factor $M = 1000$ and internal efficiency $\eta_r = 0.95$ the same type-II link with cascaded sources reduces this to 31 dB if the standard BSM protocol is used. This is further reduced to 19 dB if the ABSM protocol is employed, enabling a type-II link which is potentially comparable to a standard type-I elementary link when the latter has implementation constraints as in a satellite-assisted entanglement distribution application.

VI. CONCLUSION

In the absence of high-rate, environmentally robust, deterministic sources of entangled photon pairs, sources based on PDC remain one of the most promising candidates for high-rate entanglement distribution, particularly for satellite-assisted links. However, multiphoton noise presents a significant limitation to the performance of entanglement swapping links based on PDC. Previous attempts to address this issue were based on the use of PNR detection to identify and discard multiphoton emissions [8,11]. By taking advantage of quantum correlations present in the four-photon term of the entangled TMSV state, the ABSM protocol introduced in this paper is a technique which suppresses double-pair noise from PDC-based entangled pair sources which does not rely on PNR detection. Furthermore, the protocol can be employed in conjunction with other techniques such as cascaded PDC sources to improve the double-pair suppression afforded by PNR (Sec. V). The multiphoton noise suppression provided by the protocol analyzed in this work applies to any links using entangled pair sources with stimulated multiphoton emissions represented by a TMSV state.

Specifically, the ABSM protocol was shown to eliminate the dominant quadratic growth of multiphoton errors with the number of elementary links ℓ in repeater chains with PDC sources, yielding a gain in elementary link efficiency which grows quadratically with the number of elementary links in the chain (25)–(31). The analysis also introduced a new calculus for evaluating key observables of the quantum state produced by repeater chains of arbitrary length (Sec. III). In particular, a compact closed-form expression for the Bell state fidelity was presented including multiphoton terms (25). This calculus was also employed to obtain analytical calculations of the optimal emission probabilities and maximum efficiency for concatenated entanglement swapping links with imbalanced channel losses.

Finally, it was shown that the ABSM protocol yields a 12 dB gain for type-II elementary entanglement distribution links with cascaded PDC sources. Combined with the multipair suppression provided by PNR in the cascaded sources, it was shown that with sufficient multiplexing, such sources can enable a type-II elementary link with performance comparable to a standard type-I link. Although at present the largest multiplexed PDC sources that have been demonstrated consist of no more than approximately ten spatially multiplexed sources [22], such highly multiplexed sources constitute an engineering task for ground-based technology which can reduce flight system complexity for satellite-assisted entanglement distribution.

[1] P. Kómár, E. M. Kessler, M. Bishof, L. Jiang, A. S. Sørensen, J. Ye, and M. D. Lukin, A quantum network of clocks, Nat. Phys. **10**, 582 (2014).

[2] B. C. Nichol, R. Srinivas, D. P. Nadlinger, P. Drmota, D. Main, G. Araneda, C. J. Ballance, and D. M. Lucas, An elementary quantum network of entangled optical atomic clocks, Nature (London) **609**, 689 (2022).

[3] Z. Zhang and Q. Zhuang, Distributed quantum sensing, Quantum Sci. Technol. **6**, 043001 (2021).

[4] D. Gottesman, T. Jennewein, and S. Croke, Longer-Baseline Telescopes Using Quantum Repeaters, Phys. Rev. Lett. **109**, 070503 (2012).

[5] M. Mohageg, L. Mazzarella, C. Anastopoulos, J. Gallicchio, B.-L. Hu, T. Jennewein, S. Johnson, S.-Y. Lin, A. Ling, C. Marquardt, M. Meister, R. Newell, A. Roura, W. P. Schleich, C. Schubert, D. V. Strekalov, G. Vallone, P. Villoresi, L. Wörner, N. Yu *et al.*, The deep space quantum link: Prospective fundamental physics experiments using long-baseline quantum optics, EPJ Quantum Technol. **9**, 25 (2022).

[6] N. Sinclair, E. Saglamyurek, H. Mallahzadeh, J. A. Slater, M. George, R. Ricken, M. P. Hedges, D. Oblak, C. Simon, W. Sohler, and W. Tittel, Spectral Multiplexing for Scalable Quantum Photonics using an Atomic Frequency Comb Quantum Memory and Feed-Forward Control, Phys. Rev. Lett. **113**, 053603 (2014).

[7] N. Sangouard, C. Simon, H. de Riedmatten, and N. Gisin, Quantum repeaters based on atomic ensembles and linear optics, Rev. Mod. Phys. **83**, 33 (2011).

[8] S. Guha, H. Krovi, C. A. Fuchs, Z. Dutton, J. A. Slater, C. Simon, and W. Tittel, Rate-loss analysis of an efficient quantum repeater architecture, Phys. Rev. A **92**, 022357 (2015).

[9] M. Pant, H. Krovi, D. Englund, and S. Guha, Rate-distance tradeoff and resource costs for all-optical quantum repeaters, Phys. Rev. A **95**, 012304 (2017).

[10] H. Krovi, S. Guha, Z. Dutton, J. A. Slater, C. Simon, and W. Tittel, Practical quantum repeaters with parametric down-conversion sources, Appl. Phys. B **122**, 52 (2016).

[11] P. Dhara, S. J. Johnson, C. N. Gagatsos, P. G. Kwiat, and S. Guha, Heralded Multiplexed High-Efficiency Cascaded Source of Dual-Rail Entangled Photon Pairs Using Spontaneous Parametric Down-Conversion, Phys. Rev. Appl. **17**, 034071 (2022).

[12] N. Sangouard, C. Simon, B. Zhao, Y.-A. Chen, H. de Riedmatten, J.-W. Pan, and N. Gisin, Robust and efficient quantum repeaters with atomic ensembles and linear optics, Phys. Rev. A **77**, 062301 (2008).

[13] Y. Yu, F. Ma, X.-Y. Luo, B. Jing, P.-F. Sun, R.-Z. Fang, C.-W. Yang, H. Liu, M.-Y. Zheng, X.-P. Xie, W.-J. Zhang, L.-X. You, Z. Wang, T.-Y. Chen, Q. Zhang, X.-H. Bao, and J.-W. Pan, Entanglement of two quantum memories via fibres over dozens of kilometres, Nature (London) **578**, 240 (2020).

[14] M. Takeoka, R.-B. Jin, and M. Sasaki, Full analysis of multiphoton pair effects in spontaneous parametric down conversion based photonic quantum information processing, New J. Phys. **17**, 043030 (2015).

[15] A. Khalique, W. Tittel, and B. C. Sanders, Practical long-distance quantum communication using concatenated entanglement swapping, Phys. Rev. A **88**, 022336 (2013).

[16] P. Kok and S. L. Braunstein, Postselected versus non-postselected quantum teleportation using parametric down-conversion, Phys. Rev. A **61**, 042304 (2000).

[17] A. Lamas-Linares, J. C. Howell, and D. Bouwmeester, Stimulated emission of polarization-entangled photons, Nature (London) **412**, 887 (2001).

[18] G. A. Durkin, C. Simon, and D. Bouwmeester, Multiphoton Entanglement Concentration and Quantum Cryptography, Phys. Rev. Lett. **88**, 187902 (2002).

[19] See Supplemental Material at http://link.aps.org/supplemental/10.1103/PhysRevA.108.022609 for details.

[20] E. Shchukin and P. van Loock, Optimal Entanglement Swapping in Quantum Repeaters, Phys. Rev. Lett. **128**, 150502 (2022).

[21] J. Floyd and P. Kwiat, in *Quantum Computing, Communication, and Simulation III*, edited by P. R. Hemmer and A. L. Migdall, SPIE Proc. Vol. 12446 (SPIE, Bellingham, 2023), p. 124460L.

[22] E. Meyer-Scott, C. Silberhorn, and A. Migdall, Single-photon sources: Approaching the ideal through multiplexing, Rev. Sci. Instrum. **91**, 041101 (2020).